
HiRes-LLaVA: Restoring Fragmentation Input in High-Resolution Large Vision-Language Models

Runhui Huang^{1*} Xinpeng Ding^{3*} Chunwei Wang² Jianhua Han²
Yulong Liu² Hengshuang Zhao⁴ Hang Xu² Lu Hou² Wei Zhang² Xiaodan Liang^{1†}
¹Shenzhen campus of Sun Yat-sen University ²Huawei Noah's Ark Lab
³The Hong Kong University of Science and Technology ⁴The University of Hong Kong

Abstract

High-resolution inputs enable Large Vision-Language Models (LVLMs) to discern finer visual details, enhancing their comprehension capabilities. To reduce the training and computation costs caused by high-resolution input, one promising direction is to use sliding windows to slice the input into uniform patches, each matching the input size of the well-trained vision encoder. Although efficient, this slicing strategy leads to the fragmentation of original input, *i.e.*, the continuity of contextual information and spatial geometry is lost across patches, adversely affecting performance in cross-patch context perception and position-specific tasks. To overcome these shortcomings, we introduce **HiRes-LLaVA**, a novel framework designed to efficiently process any size of high-resolution input without altering the original contextual and geometric information. HiRes-LLaVA comprises two innovative components: (i) a SliceRestore adapter that reconstructs sliced patches into their original form, efficiently extracting both global and local features via down-up-sampling and convolution layers, and (ii) a Self-Mining Sampler to compresses the vision tokens based on themselves, preserving the original context and positional information while reducing training overhead. To assess the ability of handling context fragmentation, we construct a new benchmark, EntityGrid-QA, consisting of edge-related and position-related tasks. Our comprehensive experiments demonstrate the superiority of HiRes-LLaVA on both existing public benchmarks and on EntityGrid-QA, particularly on document-oriented tasks, establishing new standards for handling high-resolution inputs.

1 Introduction

Recent progress in Large Vision-Language Models (LVLMs) [1, 35, 34, 37, 46, 82] has significantly enhanced capabilities in vision-language tasks, fostering improved understanding, reasoning, and interaction. Early LVLMs [34, 82, 44] processed images at low resolutions, typically 224×224 , which hindering their ability to capture detailed visual information. This limitation often results in inaccurate recognition of objects and their contextual relationships within images [17, 41].

Enhancing the high-resolution capabilities of LVLMs presents substantial challenges, *i.e.*, training visual encoders to handle high-resolution inputs requires significant computational resources as well as struggling with handling arbitrary image sizes [3, 11]. Recent advances have introduced resource-efficient methods to improve the input resolution of LVLMs. One effective strategy involves using a sliding window technique [41, 73, 49] to segment high-resolution images into smaller patches. These patches are then processed by a visual encoder that has been trained on lower-resolution inputs, maintaining computational efficiency while enhancing detail capture.

*Equal contribution

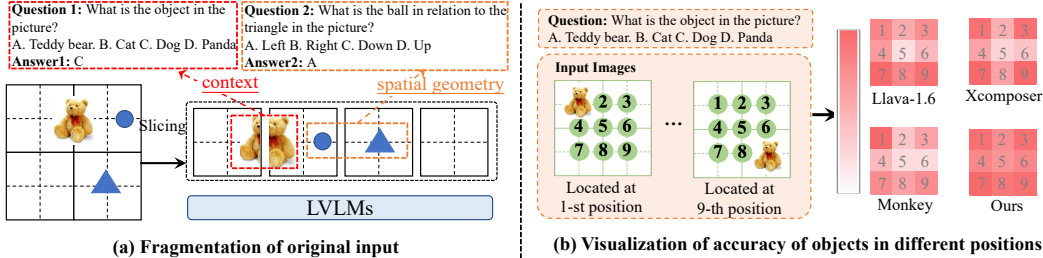


Figure 1: **(a) Fragmentation of the original input.** Current slicing-based LVLMs would disrupt the context and spatial geometry. **(b) Visualization of the accuracy of objects in different positions.** We test images with a bear positioned in nine different locations using various LVLMs. Note that the green circles with number here are only for illustration and not presented for LVLMs. By comparing the average accuracies for these positions, results indicate that bears straddling slices typically show reduced accuracy with existing SOTA models [45, 41, 80]. In contrast, our method maintains consistent accuracy across all positions.

Although effective, this slicing approach leads the fragmentation of the original input, leading to the problems such as: **(i) Disruption of Context.** Slicing the entire image can alter the original context, particularly when an object is located at the edge of two slices; **(ii) Impairment of Spatial Geometry.** Slicing disrupts the inherent spatial geometry, complicating tasks that rely on positional relationships, such as identifying objects adjacent to specific regions; see details in Fig. 1 (a). Furthermore, existing approaches [73, 49] generally use a sampler, such as Q-Former [35], to reduce the long context caused by high-resolution input. However, this Q-Former like sampler utilizes a fixed number of queries to compress and capture visual features through a cross-attention mechanism, suffering from problems, *e.g.*, lacking position information and high training overhead.

In this paper, we propose HiRes-LLaVA, an efficient approach to integrating high-resolution data into LVLMs without disrupting the original context and spatial geometry. As illustrated in Fig.1(b), our method maintains consistent accuracy even when objects are positioned across different slices. HiRes-LLaVA utilizes a new SliceRestore Adapter to combine sliced low-resolution patch features into a high-resolution feature map, preserving the image’s complete context and spatial information. This map is processed through dual parallel fusion modules to capture both global and local information. The enhanced high-resolution map is then segmented back into small patches. The SliceRestore Adapter is a lightweight module that can be seamlessly integrated into any attention layer of the low-resolution vision encoder, enabling efficient fine-tuning without altering pre-trained parameters. Furthermore, we introduce a self-mining sampler that uses average pooled sliced patches as queries. Unlike fixed learnable query-based methods, our self-mining sampler preserves the original context and positional information while optimizing efficiently.

To evaluate our proposed method, besides 11 public benchmarks, we also introduce a new benchmark named EntityGrid-QA. This benchmark is specifically designed to include identification, position, and counting tasks, which are critical for further assessing the ability of VLMs to handle context fragmentation resulting from slicing approaches. Comprehensive experiments show that our HiRes-LLaVA not only achieves superior performance on existing public benchmarks but also significantly outperforms state-of-the-art LVLMs on our newly introduced EntityGrid-QA.

2 Related Works

2.1 Large Vision-Language Model

Leveraging pre-trained Large Language Models (LLMs) such as LLaMA [71] and Vicuna [13], Large Vision-Language Models (LVLMs) have demonstrated substantial advancements across various domains including general image/video understanding [36, 35, 82, 1, 8, 79, 37], medical analysis [34], and autonomous driving [17, 74]. These models primarily encode vision features to be understood by LLMs using tools like CLIP-ViT [18, 61], pre-trained via contrastive learning with vast image-text pairs [63] to align visual embeddings with language. Subsequently, visual embeddings are transformed to match the dimensionality of LLMs through a visual projector, categorized into: (i)

learned queries such as the perceiver resampler [1] or Q-Former [35, 82] that use fixed queries for capturing features via cross-attention, and (ii) MLP modules, exemplified by the LLaVA series [46]. Recent efforts have explored combining diverse visual features from sources like DINO-V2 [60] and SAM [28] with CLIP-ViT to enrich visual representation [62, 42]. However, the dependency on CLIP-ViT, which requires images of fixed resolution (e.g., 336×336), restricts handling higher resolutions or varying aspect ratios, thereby limiting performance in fine-grained tasks.

2.2 High Resolution Large Vision-Language Model

To discern fine-grained visual details from high-resolution inputs, an intuitive approach is to split images into patches and project them using linear layers, treating these as a sequence for input into Large Vision-Language Models (LVLMs) [4, 32]. While this eliminates the need for an image encoder, it often results in insufficient visual representation, leading to increased training costs and suboptimal performance. Alternatively, Up-Resize methods such as Qwen-VL [3] adapt the positional embeddings of Vision Transformers (ViT) from 224×224 to 448×448 and include an additional training phase to fine-tune the ViT. However, this adaptation may alter the original visual position encoding from CLIP-ViT [61], potentially degrading visual representation. Dual-branch approaches introduce a high-resolution branch with lightweight convolutional networks to manage high-resolution inputs but require additional training data and parameters [22, 17, 52, 38]. Slicing-based methods offer a compromise by using slicing windows to divide the high-resolution image into patches that match the input size of a pre-trained vision encoder, maintaining efficiency in parameter use and training data while still achieving competitive performance [41, 73]. However, they suffer from "Context Fragmentation", where the continuity of contextual information across patches is damaged, impacting tasks that require cross-patch context and spatial relationships. In this paper, we propose HiRes-LLaVA, a novel technique designed to seamlessly integrate global-local high-resolution details into LVLMs without disrupting the original context or spatial geometry, effectively addressing the issue of Context Fragmentation.

3 Method

The overall framework of HiRes-LLaVA is shown in Fig. 2(a). First, the original image is resized and padded to a low resolution (typically 224×224) and processed by the pre-trained CLIP-ViT[61], producing global features. To capture high-resolution details, the image is split into slices, each matching the CLIP-ViT input size. These slices are processed by a shared CLIP-ViT with the proposed SliceRestore adapter (Section 3.1), yielding slice features. The slice features are then fed into a shared self-mining sampler to reduce token length, resulting in compressed features. These compressed features, along with text instruction embeddings, are concatenated and fed into the LLM to generate the response. Importantly, we keep the vision encoder (CLIP-ViT) and LLM parameters frozen, training only the proposed SliceRestore adapter, the self-mining sampler and LoRA.

3.1 SliceRestore Adapter

As depicted in Fig. 2 (b), the SliceRestore adapter is integrated into the self-attention layer of CLIP-ViT. We denote the slice features in the l -th layer of ViT as $\{\mathbf{P}_i\}_{i=1}^N$ with $\mathbf{P}_i \in \mathbb{R}^{L \times D}$, where N is the number of slices, $L = H \times W$ is the token length, and D is the feature dimension. Each slice feature is processed individually by the self-attention layer, $\text{Self-Attn}(\mathbf{P}_i)$, which can fragment context and disrupt image geometry (see Fig. 1 (a)). Although low-resolution inputs contain the overall information, small objects in slices are still difficult to perceive. A naive approach would be concatenating slice features for self-attention, but this incurs quadratic computation costs.

In this paper, we propose the SliceRestore adapter to efficiently capture complete information from high-resolution inputs. This is formulated as:

$$\{\hat{\mathbf{P}}_i\}_{i=1}^N = \{\text{Self-Attn}(\mathbf{P}_i)\}_{i=1}^N + \{\bar{\mathbf{P}}_i\}_{i=1}^N, \quad (1)$$

where:

$$\{\bar{\mathbf{P}}_i\}_{i=1}^N = \text{SRA}(\{\mathbf{P}_i\}_{i=1}^N), \quad (2)$$

and SRA represents the proposed SliceRestore adapter.

The SliceRestore adapter has three main steps to restore complete semantics from slice features:

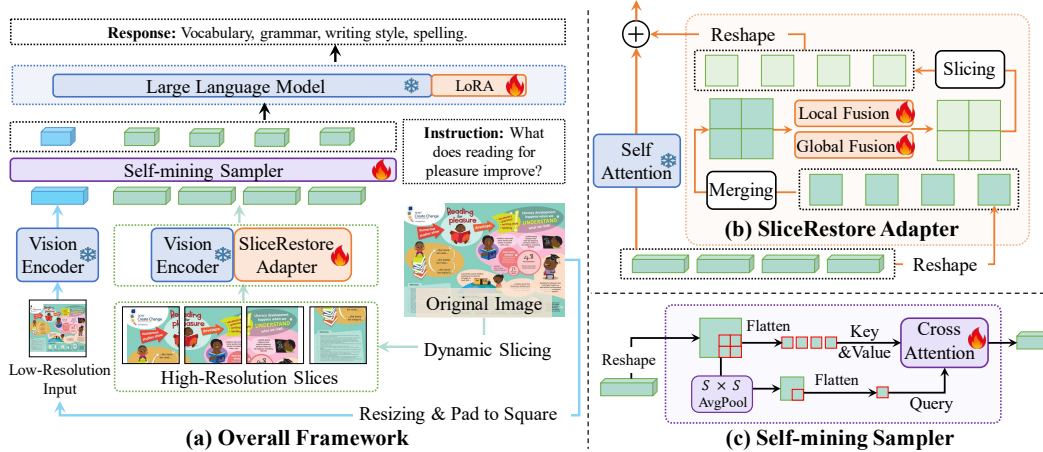


Figure 2: **(a) Overall framework of HiRes-LLaVA.** The vision encoding consists of two branches: one for low-resolution images processed by CLIP-ViT to extract global features, and another for high-resolution images to capture fine-grained details. **(b) SliceRestore Adapter.** This component restores sliced features into a whole feature by capturing both local and global information, then splits the whole feature back into slices. **(c) Self-Mining Sampler.** This component compresses vision token numbers to reduce computation and memory costs by using downsampled sliced features as queries and the original sliced features as keys and values. Both low-resolution image input and each high-resolution slice are compressed by the same self-mining sampler.

1. Merging: Each slice feature \mathbf{P}_i is first reshaped into $\mathbf{H}_i \in \mathbb{R}^{H \times W \times D}$. These reshaped slice features, $\{\mathbf{H}_i\}_{i=1}^N$, are then merged to form the original input’s features $\mathbf{F} \in \mathbb{R}^{(m * W) \times (n * H) \times D}$. m and n indicates the number of rows and columns of slices, respectively. N is equal to $m * n$

2. Capturing: We use two fusion modules for extracting both local and global information from \mathbf{F} . The local fusion module uses a single layer depth-wise convolution with 3×3 kernel to efficiently capture local details and retain image-related biases. The global fusion module employs self-attention to capture global context. Given the quadratic computation cost of self-attention, we first downsample \mathbf{F}^l to a smaller size, $(m * W_1) \times (n * H_1)$ ($W_1 < W$ and $H_1 < H$), perform self-attention, and then up-sample back to the original size. The enhanced whole feature $\bar{\mathbf{F}}$ is obtained by element-wise addition of the outputs from the local and global fusion modules:

$$\bar{\mathbf{F}} = \underbrace{\text{Depth-Wise Conv}(\mathbf{F})}_{\text{local fusion}} + \underbrace{\text{Up}(\text{Self-Attn}(\text{Down}(\mathbf{F})))}_{\text{global fusion}}. \quad (3)$$

3. Slicing: Finally, the enhanced whole feature $\bar{\mathbf{F}}$ is sliced back into the original slice format, resulting in $\{\bar{\mathbf{P}}_i\}_{i=1}^N$, where $\bar{\mathbf{P}}_i \in \mathbb{R}^{L \times D}$.

This process allows model to capture the complete semantics from high-resolution inputs while maintaining computational efficiency.

3.2 Self-Mining Sampler

High-resolution images necessitate processing significantly more visual tokens, contributing to a substantial part of the computational load. Existing solutions, such as Q-Former [35], utilize a fixed number of queries to compress and capture visual features through a cross-attention mechanism. While this method effectively captures visual information regardless of image resolution in a computationally affordable manner, it suffers from several limitations: **(i) Lacking Positional Information.** Learned queries lose positional information, degrading performance in tasks requiring spatial relationships and precise localization. **(ii) High Training Overhead.** Training Q-Former-like resamplers requires more data and longer training times to convert visual features into learnable queries, posing challenges in data-scarce domains.

To address the issues, we propose a self-mining sampler, as shown in Fig. 2(c). Specifically, we reshape the one-dimensional output vision tokens of the vision encoder (e.g., CLIP-ViT), $\mathbf{P} \in \mathbb{R}^{L \times D}$,

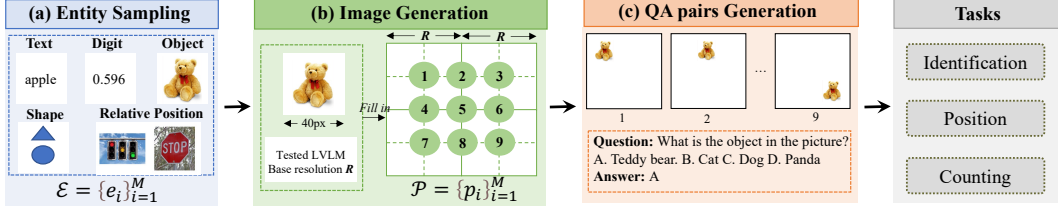


Figure 3: **Construction process of our proposed EntityGrid-QA benchmark.** There are three steps: **(a) Entity Sampling.** Select one or two entities from the pre-defined entity set; **(b) Image Generation.** Put the selected entities in one position sampled from the nine pre-defined positions of the blank image, we can obtain the generated images. Note that the dash and solid lines in (b) are for illustration purposes only, and not presented to models. **(c) QA pairs Generation.** Based on the generated images, entity category and positions, we can automatically generate the question-answer pairs (QAs). We totally construct three different tasks, *i.e.*, identification, position and counting.

into a two-dimensional form, $H \times W \times D$, where $L = H \times W$. After applying average-pooling with kernel size $S \times S$, we obtain $\mathbf{P}^c \in \mathbb{R}^{H_2 \times W_2 \times D}$, where $W_2 < W$ and $H_2 < H$. Next, we compute the final compressed tokens using cross-attention, $\text{Cross-Attn}(\mathbf{P}^c, \mathbf{P})$, with \mathbf{P}^c as the query and \mathbf{P} as the key and values. Compared with fixed learnable query-based methods, our self-mining sampler compresses the vision tokens based on themselves, preserving the original context and positional information while reducing training overhead.

3.3 Dynamic High Resolution Slicing

Pre-trained visual encoders, utilized across supervised, self-supervised, and vision-language pretraining, predominantly reshape images into squares by cropping or padding. This approach, however, struggles with non-square images prevalent in real-world scenarios, particularly failing to preserve detail or loss information in images with extreme aspect ratios. The current solution of high-resolution images input in large vision-language models involves slicing these images into pre-trained model-compatible slices based on pre-defined aspect ratio candidates, which does not accommodate the diversity of real-world imagery effectively [45, 76, 41].

In contrast, HiRes-LLaVA dynamically slices high-resolution images without predefining aspect ratio candidates which enables any aspect ratio image inputs. We set a maximum slice count M , allowing an image to automatically select an optimal bounding box by calculating the necessary m rows and n columns based on the base resolution:

$$m = \left\lceil \frac{H}{r} \right\rceil, n = \left\lceil \frac{W}{r} \right\rceil.$$

Where r is the base resolution in pretrained vision encoder. $\lceil x \rceil$ denotes the ceiling function of x , which round up the x to the smallest integer greater than itself if x is decimal.

This approach adapts to the image’s aspect ratio, only quadrupling the number of slices by scaling $2 \times$ of m and n if “ $4 * m * n$ ” does not exceed M , ensuring detailed preservation without overwhelming the model. Our input to the language model includes a low-resolution overview and multiple high-resolution slices, differentiated by three types of separators to maintain clarity in (1) between the low-resolution image and high-resolution slices, (2) between high resolutions slices and (3) the end of each slice row.

3.4 EntityGrid-QA Benchmark

Existing benchmarks, particularly document-related datasets, can evaluate the fine-grained understanding of LLMs. However, these benchmarks are inadequate for assessing the ability to handle fragmented inputs, as filtering slicing-related questions is time-consuming and labour-intensive. Therefore, we introduce a new benchmark named EntityGrid-QA to better assess LLMs’ ability to handle fragmentation.

Construction Process. As shown in Fig. 3, the construction process of EntityGrid-QA consists of three main steps: Entity Sampling, Image Generation, and QA Pairs Generation. Each step is detailed as follows:

(a) Entity Sampling. We first construct one entity set which includes various types such as Text (e.g., "apple"), Digit (e.g., "0.596"), Object (e.g., a teddy bear), Shape (e.g., triangle, circle), and Relative Position (e.g., traffic lights, stop sign), as shown in Fig. 3 (a). Then, we select several entities from a predefined entity set, which can be denoted as $\mathcal{E} = \{e_i\}_{i=1}^M$, where e_i is the i -th entity and M is the total number selected entities.

(b) Image Generation. The selected entities \mathcal{E} are positioned in nine predefined positions (labeled 1 to 9) within a blank image I using a 3x3 grid layout, as shown in Fig. 3 (b). The resolution of the blank image is set to $2R$, where R is the base resolution for existing LVLMS, e.g., 224×224 . In this way, each I would be divided into four slices during inference, and each slice would match the input size of well-pretrained vision encoder, without the requirement of additional operations, e.g., resize and padding. Note that our HiRes-LLaVA can process any number of slices, however some existing LVLMS, i.e., LLaVA-1.6 [44] can only receive four slices as input. Hence, for a fair comparison, we only generate the images with a fixed resolution $2R$. We denote the selected positions as $\mathcal{P} = \{p_i\}_{i=1}^M, p_i \in [1, 9]$, where p_i is the position for e_i .

(c) QA Pairs Generation. For more comprehensive evaluation, we define three different tasks, i.e., Identification, Position and Counting, where each task has a specific question prompt, i.e., $Q_{\text{ident}}, Q_{\text{pos}}$ and Q_{count} , as follows: $Q_{\text{ident}} = \text{"What is the object in the picture?"}$, $Q_{\text{pos}} = \text{"Where is } e_i \text{ at } e_j \text{ in the picture?"}$ and $Q_{\text{count}} = \text{"How many } e_i \text{ are in the picture?"}$. Based on the generated images I as well as its corresponding entity \mathcal{E} and the question prompt Q , we can automatically generate questions, and the answer can be obtain by positions \mathcal{P} , e.g., the relative position of two objects e_i and e_j can be caculated by their positions p_i and p_j . As shown in Fig. 3 (c), the generated question-answer pairs are in a multiple choice questions format. Examples of our benchmark are provided in Appendix.

Evaluation Metric. To evaluate the ability to handle the fragmentation, we introduce a new metric that measure the precision discrepancies between entity located at the edge positions ($\mathcal{P}_{\text{edge}} = \{2, 4, 5, 6, 8\}$) and other locations ($\mathcal{P}_{\text{center}} = \{1, 3, 7, 9\}$), defined as:

$$\text{Discrepancy}_1 = \frac{\sum_{p \in \mathcal{P}_{\text{edge}}} A_p / |\mathcal{P}_{\text{edge}}|}{\sum_{p \in \mathcal{P}_{\text{center}}} A_p / |\mathcal{P}_{\text{center}}|}, \quad (4)$$

$$\text{Discrepancy}_2 = \frac{\sum_{p \in \mathcal{P}_{\text{edge}}} A_p / |\mathcal{P}_{\text{edge}}| - \sum_{p \in \mathcal{P}_{\text{center}}} A_p / |\mathcal{P}_{\text{center}}|}{\sum_{p \in \mathcal{P}_{\text{center}}} A_p / |\mathcal{P}_{\text{center}}|}, \quad (5)$$

where A_p is the average accuracy of three tasks when entities located at the position p , $|\cdot|$ is the number of elements in the set.

4 Experiment

4.1 Implementation Details

We utilize the CLIP-ViT-L/14-224px and CLIP-ViT-L/14-336px as the vision encoders, and Vicuna-7B-v1.5 as LLM. We adopt a two-stage training approach following LLaVA [47], including the pre-training stage and the instruction tuning stage. During pre-training, only the self-mining sampler is trainable. The batch size is 256, and the learning rate is 1e-3. In the instruction tuning stage, the SliceRestore adapter, self-mining sampler, and LoRA parameters [23] in LLM are trained. Four SliceRestore adapterare applied in the 19th to 22nd layers of the vision encoder. The batch size of the instruction tuning stage is 128. The LoRA has a rank of 128 and an alpha of 256. The learning rate of the LoRA parameters is 2e-4, and the learning rate of the rest of the trainable parameters, including the SliceRestore Adapter, is 2e-5. We adopt AdamW [50] as the optimizer with $\beta_1 = 0.9$ and $\beta_2 = 0.95$ to stabilize the training in the instruction tuning stage. In both two stages, the learning rates are warmed up for the first 0.03 epochs and then adjusted by a cosine scheduler in the remaining training. We don't apply any weight decay in the training. The maximum number of slices M is set to 16. All models are trained two days on 64 NVIDIA V100 GPUs under FP16. Regarding the training data, we gather public datasets to augment the original LLaVA dataset. In the pretraining stage, we collect 1.6M data, including 1.2M caption data and 0.4M OCR data. To construct a large instruction

Model	LLM	MaxRes	Doc					General		Comprehensive		
			VQA-text	ChartQA	DocVQA	InfoVQA	STVQA	AI2D	ScienceQA	LLaVA-W	MMBench	POPE
General LVLMs (normal resolution)												
InstructBLIP [15]	Vicuna-7B	224x224	50.1	5.3	4.5	16.4	-	-	-	36.0	-	-
Qwen-VL [3]	Qwen-7B	448x448	63.8	65.7	65.1	35.4	59.1	55.9	67.1	-	38.2	-
Qwen-VL-Chat [3]	Qwen-7B	448x448	61.5	66.3	62.6	-	-	57.7	68.2	-	60.6	-
LLaVA-1.5 [44]	Vicuna-7B	336x336	58.2	18.2*	-	-	38.1	54.8*	66.8	59.6*	64.3	85.9
LLaVA-1.5 [44]	Vicuna-13B	336x336	61.3	18.2*	-	-	-	59.5*	71.6	66.1*	67.7	85.9
mPLUG-Owl2 [77]	LLaMA-7B	224x224	58.2	-	-	-	-	-	68.7	-	64.5	86.2
Document LVLMs												
Donut [27]	-	2560x1920	43.5	41.8	67.5	11.6	43.5	-	-	-	-	-
DocPedia [19]	Vicuna	2560x2560	60.2	46.9	47.1	15.2	45.5	-	-	-	-	-
mPLUG-DocOwl [75] †	Vicuna	-	52.6	57.4	62.2	38.2	-	-	-	-	-	-
UReader [76]	LLaMA-7B	896x1120	57.6	59.3	65.4	42.2	57.6	-	-	-	-	-
TextMonkey [49]	QWen-7B	896	65.9	65.5	71.5	28.2	68.0	-	-	-	-	-
TextMonkey+ [49]	QWen-7B	896	64.3	66.9	73.0	28.6	65.6	-	-	-	-	-
General LVLMs (high resolution)												
Monkey [41] †	QWen-7B	1344x896	67.6	65.1	66.5	36.1	67.7	57.9	69.4	-	-	-
Mini-Gemini [39]	Vicuna-7B	672	68.4	-	-	-	-	-	-	-	65.8	-
LLaVA-UHD [73]	Vicuna-13B	672x1008	67.7	-	-	-	-	-	72.0	-	68.0	89.1
LLaVA-NeXT	Vicuna-7B	672	64.9	54.8*	-	-	-	66.6	70.2	72.3*	67.4	86.5
HiRes-LLaVA-224px †	Vicuna-7B	896x896	62.5	61.2	68.0	43.5	62.8	68.9	84.2	76.8	70.4	86.5
HiRes-LLaVA-336px †	Vicuna-7B	1344x1344	65.4	61.5	74.7	48.0	65.8	69.7	84.1	78.2	70.5	87.3

Table 1: **Quantitative results on 11 popular benchmarks.** The suffix ‘-224px’ and ‘-336px’ mean the vision encoders are CLIP-L/14-224px and CLIP-L/14-336px. ‘MaxRes’ means the maximum resolution supported. ‘Doc’, ‘General’ and ‘Comprehensive’ indicate the document-related VQA, general VQA and comprehensive benchmarks. *’ denotes the results evaluated by Imms-eval [33]. Methods with 13B LLMs are marked in gray. ‘†’ means using LoRA [23] to finetune LLM.

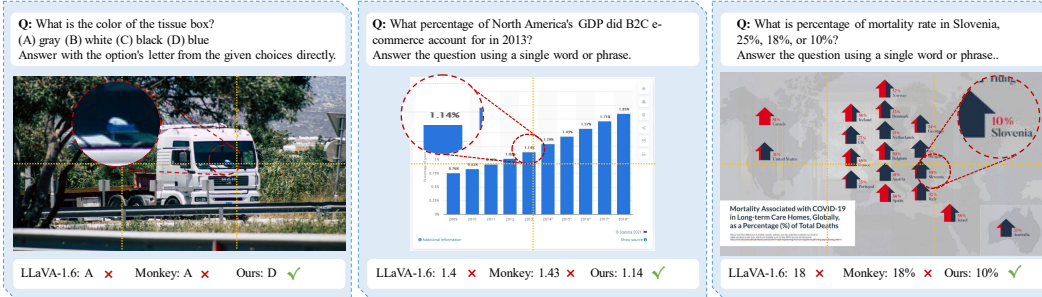


Figure 4: **The visualization comparison with the state-of-the-art methods.** Dash lines are only illustrated for the slice clarify, not presented to LVLMs.

tuning dataset that covers a wide range of tasks, we also collect 1.5M data from open-source datasets. Please refer to the Appendix for more details.

4.2 Experimental Setting

We introduce experimental settings including the benchmarks and the compared LVLMs.

Benchmarks. We adopt 11 popular benchmarks to evaluate our models on five document-related VQA benchmarks, including VQA-text[67], ChartQA test set [55], DocVQA test set [57], InfoVQA test set [56], STVQA test set [5], two general VQA benchmarks [26, 51], including AI2D [26], ScienceQA [51], and four comprehensive benchmarks, including LLaVA-in-the-wild (LLaVA-W) [47], MMBench [48], POPE [40] and HallusionBench [21].

LVLMs. We compare our model with SOTA LVLMs. (1) General baselines, *i.e.*, InstructBLIP [15], Qwen-VL [3], LLaVA-1.5 [44], mPLUG-Owl2 [77], Monkey [41], Mini-Gemini [39], LLaVA-UHD [73] and LLaVA-NeXT [45], as representative general baselines. (2) Document LVLMs, *i.e.*, Donut [27], DocPedia [19], UReader [76], mPLUG-Docowl [75], TextMonkey [49].

4.3 State-of-the-art Comparison

General Benchmarks. Table 1 reports the performance comparison of our methods against state-of-the-art approaches on 11 benchmarks. Unexpectedly, our method utilizing LoRA fine-tuning [23] surpasses well-established LVLMs that require substantial data and extensive full fine-tuning, underscoring our model’s efficiency and effectiveness. Notably, although both our model and Monkey [41] employ LoRA, Monkey is initialized from the pre-trained Qwen model [2], while our model is trained

Model	Accuracy _{mean} ↑	Accuracy _{std} ↓	Accuracy _{edge} ↑	Accuracy _{center} ↑	Discrepancy ₁ ↑	Discrepancy ₂ ↓
LLaVA-Next [45]	0.6170	0.0031	0.5819	0.6624	0.8784	0.1215
Monkey [41]	0.6000	0.0015	0.5739	0.6324	0.9075	0.0924
Xcomposer [80]	0.6311	0.0025	0.5919	0.6799	0.8705	0.1294
HiRes-LLaVA-224px	0.6400	0.0009	0.6200	0.6650	0.9323	0.0676
HiRes-LLaVA-336px	0.6300	0.0009	0.6100	0.6550	0.9312	0.0687

Table 2: **Comparison with the state-of-the-art methods on EntityGrid-QA.** ‘↓’ indicates lower scores are better, while ‘↑’ means higher scores are better. The suffix ‘-224px’ and ‘-336px’ mean the vision encoders are CLIP-L/14-224px and CLIP-L/14-336px, respectively. ‘Accuracy_{mean}’ and ‘Accuracy_{std}’, representing the mean and standard deviation of the average accuracy across three tasks. ‘Accuracy_{edge}’ and ‘Accuracy_{center}’ show the average accuracy for entities at \mathcal{P}_{edge} and \mathcal{P}_{center} , respectively. Discrepancy₁ and Discrepancy₂ are calculated using Eq. 4 and Eq. 5.

Components			DOC VQA				
Downsampler	SRA	Separator	VQA-Text	ChartQA	DocQA	InfoVQA	Avg.
ConcatChannel	X	X	60.3	54.4	54.8	34.3	50.9
Resampler [2]	X	X	58.8	49.8	42.8	32.6	46.0
C-Abstractor [6]	X	X	59.0	55.6	54.7	36.7	51.5
SMS	X	X	60.0	56.2	58.0	37.4	52.9
SMS	✓	X	61.5	56.9	57.6	38.4	53.6
SMS	✓	✓	61.8	58.8	59.7	41.4	55.4

Table 3: **The ablation study of different proposed modules.** ‘SMS’ and ‘SRA’ represent the Self-Mining Sampler and SliceRestore Adapter, respectively. The downsample rate of all downsampler are 4×.

from scratch, which further proves our model’s efficiency. Furthermore, our method demonstrates competitive performance against specialized document-centric LVLMs such as TextMonkey [49], proving its capability to manage document-related tasks effectively.

Fig. 4 shows a visual comparison of results generated by LLaVA-1.6 [44], Monkey [41], and our method, highlighting our superior performance, especially when the region of interest spans across slices. For example, the number 1.14 in Fig. 4 (b) is split into two slices, causing Monkey to misrecognize it as 1.4. Additionally, the slicing operation separates the year and percentage values into different slices, leading LLaVA-1.6 to incorrectly associate the 2017 percentage with 2014 due to the lack of global information. Our method, with the SliceRestore adapter capturing complete global high-resolution information, correctly predicts the answers.

EntityGrid-QA. To evaluate the ability to address input fragmentation, we compare four SOTA slicing-based LVLMs with our HiRes-LLaVA and present the results in Table 2.

From Table 2, we observe two key findings: (i) Our method performs competitively on tasks with entities at \mathcal{P}_{center} . For instance, our method scores 0.6400 in accuracy_{mean} and 0.6650 on Accuracy_{center}, compared to the best prior SOTA scores of 0.6311 and 0.6799. (ii) Our method significantly outperforms SOTAs in handling entities at \mathcal{P}_{edge} . For example, the previous SOTA, Xcomposer [80], shows a notable difference between Accuracy_{edge} and Accuracy_{center}, with 0.5919 vs. 0.6799. In contrast, our method achieves a smaller difference, with 0.6200 in accuracy_{edge} and 0.6650 on Accuracy_{center}. Additionally, the values of Discrepancy₁ and Discrepancy₂ further reflect the consistent performance of our method for both edge and center cases, surpassing existing SOTAs. In summary, our HiRes-LLaVA demonstrates superior ability to handle input fragmentation while maintaining competitive performance in center cases.

4.4 Ablation Study

In this section, we conduct ablation studies to evaluate the effect of our proposed modules. In our ablation study, we conduct the experiments on the LLaVA 1.2M data [44] with additional 79K document-oriented data in the instruction tuning stage, i.e., DocVQA [57], ChartQA [55] and InfoVQA [56].

Effect of different proposed modules. We ablate the two main components of our HiRes-LLaVA, specifically the SliceRestore adapter (SRA) and the self-mining sampler (SMS), as shown in Table 3. Our findings are as follows: Our SMS demonstrates superior performance compared to other sam-

Base Resolution	Downsample Kernel Size	Max # Token (Token/Slice)	DOC VQA				
			VQA-Text	ChartQA	DocVQA	InfoVQA	Avg.
224	2×2	1088 (64)	61.8	58.8	59.7	41.4	55.4
224	4×4	272 (16)	59.6	53.9	46.3	33.0	48.2
224	8×8	68 (4)	54.9	46.8	35.3	29.6	41.7
336	2×2	2448 (144)	63.6	58.5	65.7	40.7	57.1
336	3×3	1088 (64)	61.2	56.7	59.8	38.7	54.1
336	4×4	512 (36)	61.4	53.3	54.3	34.3	50.8

Table 4: **Effect of different downsample kernel sizes in the self-mining sampler.** ‘Downsample Kernel Size’ is $S \times S$ defined in Section 3.2. ‘Base Resolution’ indicates the base resolution of the vision encoder. ‘Max # Token’ indicates the maximum number of visual tokens, *i.e.*, $H_2 \times W_2$, as the maximum number of slices is 16.

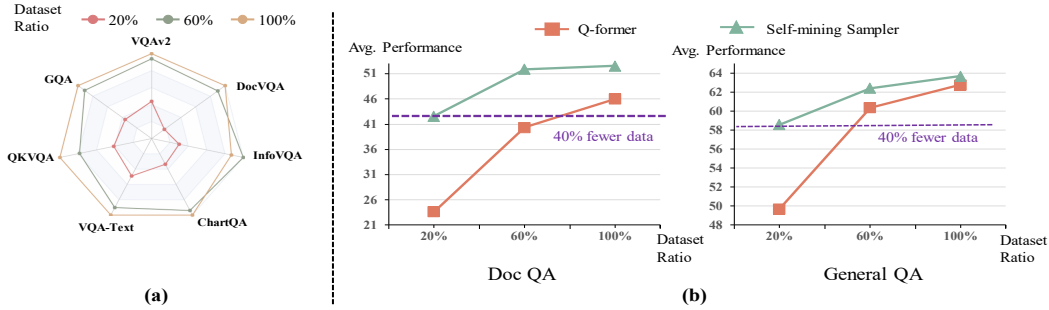


Figure 5: **(a) Ablation on data efficiency of HiRes-LLaVA.** We sample the training data mixture at ratios of 20%, 60%, and 100% and report the performance of our HiRes-LLaVA on seven benchmarks. **(b) Data efficiency comparison with Q-former and our proposed self-mining sampler (SMS).** The performance on ‘Doc QA’ is averaged from DocVQA, ChartQA and InfoVQA. The performance on ‘General QA’ is averaged from the other four benchmarks. Our SMS can use 40% fewer data to achieve competitive performance compared with Q-former, which indicates the efficiency of our method. Note that both Q-former and our SMS apply one cross-attention block.

plers, notably outperforming Resampler [2] by 6.9% on the average score across four benchmarks. Integrating the model with SRA leads to further improvements across these benchmarks. Additionally, the introduction of learnable queries to isolate slice representations, referred to as Separator, results in a 1.8% enhancement in the average score.

Ablation study of different kernel sizes in the self-mining sampler. Here we conduct the ablation study of the self-mining sampler. In Table 4, we compare the performance of the average pooling with different kernel sizes, *i.e.*, $s \times s$ in Section 3.2. The results show that as the kernel size increases, *i.e.*, the fewer vision tokens, the performance would degrade, since the information loss.

Data efficiency analysis. We evaluated the data efficiency of our method, HiRes-LLaVA, by subsampling the training data mixture at ratios of 20%, 60%, and 100%. Results in Fig. 5 (a) show that using the entire dataset achieves optimal performance. Remarkably, with only 60% of the data, performance remains above 90% of the full dataset’s level, highlighting the potential for improved data efficiency. Additionally, we compared our self-mining sampler’s efficiency against the commonly used Q-former in LVLMs. As depicted in Fig. 5 (b), our method performs competitively with Q-former even with only 20% of the data, demonstrating its effectiveness and efficiency.

5 Conclusion

In this paper, we present HiRes-LLaVA, a large visual-language model (LVLm) designed to efficiently address input fragmentation caused by current slicing-based high-resolution LVLms. To evaluate this capability, we introduce a new benchmark, EntityGrid-QA, which includes identification, position, and counting tasks. Comprehensive experimental results on 11 popular existing benchmarks and EntityGrid-QA demonstrate the effectiveness of HiRes-LLaVA. Analytical evaluation and visualization results are provided for a deeper understanding of the model’s performance.

Limitations. The samples in our constructed EntityGrid-QA are simple, lacking complex backgrounds, and the categories of entities and tasks are limited. In the future, we aim to create a more diverse dataset to better evaluate the performance of LVLMs in handling fragmented input.

References

- [1] Jean-Baptiste Alayrac, Jeff Donahue, Pauline Luc, Antoine Miech, Iain Barr, Yana Hasson, Karel Lenc, Arthur Mensch, Katherine Millican, Malcolm Reynolds, et al. Flamingo: a visual language model for few-shot learning. *Advances in Neural Information Processing Systems*, 35:23716–23736, 2022. 1, 2, 3
- [2] Jinze Bai, Shuai Bai, Shusheng Yang, Shijie Wang, Sinan Tan, Peng Wang, Junyang Lin, Chang Zhou, and Jingren Zhou. Qwen-vl: A frontier large vision-language model with versatile abilities. *arXiv preprint arXiv:2308.12966*, 2023. 7, 8, 9
- [3] Jinze Bai, Shuai Bai, Shusheng Yang, Shijie Wang, Sinan Tan, Peng Wang, Junyang Lin, Chang Zhou, and Jingren Zhou. Qwen-vl: A versatile vision-language model for understanding, localization, text reading, and beyond. *arXiv preprint arXiv:2308.12966*, 2023. 1, 3, 7
- [4] Rohan Bavishi, Erich Elsen, Curtis Hawthorne, Maxwell Nye, Augustus Odena, Arushi Somani, and Sağnak Taşlılar. Introducing our multimodal models, 2023. 3
- [5] Ali Furkan Biten, Ruben Tito, Andres Mafla, Lluís Gomez, Marçal Rusinol, Ernest Valveny, CV Jawahar, and Dimosthenis Karatzas. Scene text visual question answering. In *ICCV*, pages 4291–4301, 2019. 7, 15, 16
- [6] Junbum Cha, Wooyoung Kang, Jonghwan Mun, and Byungseok Roh. Honeybee: Locality-enhanced projector for multimodal llm. *arXiv preprint arXiv:2312.06742*, 2023. 8
- [7] Guiming Hardy Chen, Shunian Chen, Ruifei Zhang, Junying Chen, Xiangbo Wu, Zhiyi Zhang, Zhihong Chen, Jianquan Li, Xiang Wan, and Benyou Wang. Allava: Harnessing gpt4v-synthesized data for a lite vision-language model. *arXiv preprint arXiv:2402.11684*, 2024. 15, 16
- [8] Keqin Chen, Zhao Zhang, Weili Zeng, Richong Zhang, Feng Zhu, and Rui Zhao. Shikra: Unleashing multimodal llm’s referential dialogue magic. *arXiv preprint arXiv:2306.15195*, 2023. 2
- [9] Lin Chen, Jisong Li, Xiaoyi Dong, Pan Zhang, Conghui He, Jiaqi Wang, Feng Zhao, and Dahua Lin. Sharegpt4v: Improving large multi-modal models with better captions. *arXiv preprint arXiv:2311.12793*, 2023. 15, 16
- [10] Wenhui Chen, Hongmin Wang, Jianshu Chen, Yunkai Zhang, Hong Wang, Shiyang Li, Xiyu Zhou, and William Yang Wang. Tabfact: A large-scale dataset for table-based fact verification. *arXiv preprint arXiv:1909.02164*, 2019. 15, 16
- [11] Xi Chen, Xiao Wang, Lucas Beyer, Alexander Kolesnikov, Jialin Wu, Paul Voigtlaender, Basil Mustafa, Sebastian Goodman, Ibrahim Alabdulmohsin, Piotr Padlewski, et al. Pali-3 vision language models: Smaller, faster, stronger. *arXiv preprint arXiv:2310.09199*, 2023. 1
- [12] Xingyu Chen, Zihan Zhao, Lu Chen, Jiabao Ji, Danyang Zhang, Ao Luo, Yuxuan Xiong, and Kai Yu. Websrc: A dataset for web-based structural reading comprehension. In *Proceedings of the 2021 Conference on Empirical Methods in Natural Language Processing*, pages 4173–4185, 2021. 15, 16
- [13] Wei-Lin Chiang, Zhuohan Li, Zi Lin, Ying Sheng, Zhanghao Wu, Hao Zhang, Lianmin Zheng, Siyuan Zhuang, Yonghao Zhuang, Joseph E Gonzalez, et al. Vicuna: An open-source chatbot impressing gpt-4 with 90%* chatgpt quality. See <https://vicuna.lmsys.org> (accessed 14 April 2023), 2023. 2
- [14] Christopher Clark and Matt Gardner. Simple and effective multi-paragraph reading comprehension. In *ACL*, pages 845–855, 2018. 15, 16
- [15] Wenliang Dai, Junnan Li, Dongxu Li, Anthony Meng Huat Tiong, Junqi Zhao, Weisheng Wang, Boyang Li, Pascale N Fung, and Steven Hoi. Instructblip: Towards general-purpose vision-language models with instruction tuning. *NeurIPS*, 36, 2024. 7
- [16] Abhishek Das, Satwik Kottur, Khushi Gupta, Avi Singh, Deshraj Yadav, José MF Moura, Devi Parikh, and Dhruv Batra. Visual dialog. In *CVPR*, pages 326–335, 2017. 15, 16
- [17] Xinpeng Ding, Jianhua Han, Hang Xu, Wei Zhang, and Xiaomeng Li. Hilm-d: Towards high-resolution understanding in multimodal large language models for autonomous driving. *arXiv preprint arXiv:2309.05186*, 2023. 1, 2, 3
- [18] Alexey Dosovitskiy, Lucas Beyer, Alexander Kolesnikov, Dirk Weissenborn, Xiaohua Zhai, Thomas Unterthiner, Mostafa Dehghani, Matthias Minderer, Georg Heigold, Sylvain Gelly, et al. An image is worth 16x16 words: Transformers for image recognition at scale. *arXiv preprint arXiv:2010.11929*, 2020. 2
- [19] Hao Feng, Qi Liu, Hao Liu, Wengang Zhou, Houqiang Li, and Can Huang. Docpedia: Unleashing the power of large multimodal model in the frequency domain for versatile document understanding. *arXiv preprint arXiv:2311.11810*, 2023. 7
- [20] Yash Goyal, Tejas Khot, Douglas Summers-Stay, Dhruv Batra, and Devi Parikh. Making the v in vqa matter: Elevating the role of image understanding in visual question answering. In *CVPR*, pages 6904–6913, 2017. 16

- [21] Tianrui Guan, Fuxiao Liu, Xiyang Wu, Ruiqi Xian, Zongxia Li, Xiaoyu Liu, Xijun Wang, Lichang Chen, Furong Huang, Yaser Yacoob, et al. Hallusionbench: An advanced diagnostic suite for entangled language hallucination & visual illusion in large vision-language models. *arXiv preprint arXiv:2310.14566*, 2023. 7
- [22] Wenyi Hong, Weihang Wang, Qingsong Lv, Jiazheng Xu, Wenmeng Yu, Junhui Ji, Yan Wang, Zihan Wang, Yuxiao Dong, Ming Ding, and Jie Tang. Cogagent: A visual language model for gui agents, 2023. 3
- [23] Edward J Hu, Yelong Shen, Phillip Wallis, Zeyuan Allen-Zhu, Yuanzhi Li, Shean Wang, Lu Wang, and Weizhu Chen. Lora: Low-rank adaptation of large language models. *arXiv preprint arXiv:2106.09685*, 2021. 6, 7
- [24] Drew A Hudson and Christopher D Manning. Gqa: A new dataset for real-world visual reasoning and compositional question answering. In *CVPR*, pages 6700–6709, 2019. 16
- [25] Kushal Kafle, Brian Price, Scott Cohen, and Christopher Kanan. Dvqa: Understanding data visualizations via question answering. In *CVPR*, pages 5648–5656, 2018. 15, 16
- [26] Aniruddha Kembhavi, Mike Salvato, Eric Kolve, Minjoon Seo, Hannaneh Hajishirzi, and Ali Farhadi. A diagram is worth a dozen images. In *ECCV*, pages 235–251, 2016. 7, 15, 16
- [27] Geewook Kim, Teakgyu Hong, Moonbin Yim, JeongYeon Nam, Jinyoung Park, Jinyeong Yim, Wonseok Hwang, Sangdoon Yun, Dongyoon Han, and Seunghyun Park. Ocr-free document understanding transformer. In *ECCV*, 2022. 7, 15
- [28] Alexander Kirillov, Eric Mintun, Nikhila Ravi, Hanzi Mao, Chloe Rolland, Laura Gustafson, Tete Xiao, Spencer Whitehead, Alexander C. Berg, Wan-Yen Lo, Piotr Dollár, and Ross Girshick. Segment anything. *arXiv:2304.02643*, 2023. 3
- [29] Ranjay Krishna, Yuke Zhu, Oliver Groth, Justin Johnson, Kenji Hata, Joshua Kravitz, Stephanie Chen, Yannis Kalantidis, Li-Jia Li, David A Shamma, et al. Visual genome: Connecting language and vision using crowdsourced dense image annotations. *IJCV*, 123:32–73, 2017. 16
- [30] LAION. Gpt-4v dataset. <https://huggingface.co/datasets/laion/gpt4v-dataset>, 2023. 15, 16
- [31] Hugo Laurençon, Léo Tronchon, and Victor Sanh. Unlocking the conversion of web screenshots into html code with the websight dataset, 2024. 16
- [32] Bo Li, Peiyuan Zhang, Jingkang Yang, Yuanhan Zhang, Fanyi Pu, and Ziwei Liu. Otterhd: A high-resolution multi-modality model. *arXiv preprint arXiv:2311.04219*, 2023. 3
- [33] Bo Li*, Peiyuan Zhang*, Kaichen Zhang*, Fanyi Pu*, Xinrun Du, Yuhao Dong, Haotian Liu, Yuanhan Zhang, Ge Zhang, Chunyuan Li, and Ziwei Liu. Lmms-eval: Accelerating the development of large multimodal models, March 2024. 7, 15
- [34] Chunyuan Li, Cliff Wong, Sheng Zhang, Naoto Usuyama, Haotian Liu, Jianwei Yang, Tristan Naumann, Hoifung Poon, and Jianfeng Gao. Llava-med: Training a large language-and-vision assistant for biomedicine in one day. *arXiv preprint arXiv:2306.00890*, 2023. 1, 2
- [35] Junnan Li, Dongxu Li, Silvio Savarese, and Steven Hoi. Blip-2: Bootstrapping language-image pre-training with frozen image encoders and large language models. *arXiv preprint arXiv:2301.12597*, 2023. 1, 2, 3, 4
- [36] Junnan Li, Dongxu Li, Caiming Xiong, and Steven Hoi. Blip: Bootstrapping language-image pre-training for unified vision-language understanding and generation. In *International Conference on Machine Learning*, pages 12888–12900. PMLR, 2022. 2
- [37] KunChang Li, Yanan He, Yi Wang, Yizhuo Li, Wenhao Wang, Ping Luo, Yali Wang, Limin Wang, and Yu Qiao. Videochat: Chat-centric video understanding. *arXiv preprint arXiv:2305.06355*, 2023. 1, 2
- [38] Yanwei Li, Yuechen Zhang, Chengyao Wang, Zhisheng Zhong, Yixin Chen, Ruihang Chu, Shaoteng Liu, and Jiaya Jia. Mini-gemini: Mining the potential of multi-modality vision language models. *arXiv preprint arXiv:2403.18814*, 2024. 3
- [39] Yanwei Li, Yuechen Zhang, Chengyao Wang, Zhisheng Zhong, Yixin Chen, Ruihang Chu, Shaoteng Liu, and Jiaya Jia. Mini-gemini: Mining the potential of multi-modality vision language models. *arXiv preprint arXiv:2403.18814*, 2024. 7
- [40] Yifan Li, Yifan Du, Kun Zhou, Jinpeng Wang, Wayne Xin Zhao, and Ji-Rong Wen. Evaluating object hallucination in large vision-language models. In *EMNLP*, pages 292–305, 2023. 7
- [41] Zhang Li, Biao Yang, Qiang Liu, Zhiyin Ma, Shuo Zhang, Jingxu Yang, Yabo Sun, Yuliang Liu, and Xiang Bai. Monkey: Image resolution and text label are important things for large multi-modal models. *arXiv preprint arXiv:2311.06607*, 2023. 1, 2, 3, 5, 7, 8
- [42] Ziyi Lin, Chris Liu, Renrui Zhang, Peng Gao, Longtian Qiu, Han Xiao, Han Qiu, Chen Lin, Wenqi Shao, Keqin Chen, Jiaming Han, Siyuan Huang, Yichi Zhang, Xuming He, Hongsheng Li, and Yu Qiao. Sphinx: The joint mixing of weights, tasks, and visual embeddings for multi-modal large language models. 3

- [43] Fangyu Liu, Guy Emerson, and Nigel Collier. Visual spatial reasoning. *TACL*, 11:635–651, 2023. 15, 16
- [44] Haotian Liu, Chunyuan Li, Yuheng Li, and Yong Jae Lee. Improved baselines with visual instruction tuning. *arXiv preprint arXiv:2310.03744*, 2023. 1, 6, 7, 8, 15
- [45] Haotian Liu, Chunyuan Li, Yuheng Li, Bo Li, Yuanhan Zhang, Sheng Shen, and Yong Jae Lee. Llava-next: Improved reasoning, ocr, and world knowledge, January 2024. 2, 5, 7, 8, 15
- [46] Haotian Liu, Chunyuan Li, Qingyang Wu, and Yong Jae Lee. Visual instruction tuning. *arXiv preprint arXiv:2304.08485*, 2023. 1, 3
- [47] Haotian Liu, Chunyuan Li, Qingyang Wu, and Yong Jae Lee. Visual instruction tuning. *NeurIPS*, 36, 2023. 6, 7, 15, 16
- [48] Yuan Liu, Haodong Duan, Yuanhan Zhang, Bo Li, Songyang Zhang, Wangbo Zhao, Yike Yuan, Jiaqi Wang, Conghui He, Ziwei Liu, et al. Mmbench: Is your multi-modal model an all-around player? *arXiv preprint arXiv:2307.06281*, 2023. 7
- [49] Yuliang Liu, Biao Yang, Qiang Liu, Zhang Li, Zhiyin Ma, Shuo Zhang, and Xiang Bai. Textmonkey: An ocr-free large multimodal model for understanding document. *arXiv preprint arXiv:2403.04473*, 2024. 1, 2, 7, 8
- [50] Ilya Loshchilov and Frank Hutter. Decoupled weight decay regularization. *arXiv preprint arXiv:1711.05101*, 2017. 6
- [51] Pan Lu, Swaroop Mishra, Tanglin Xia, Liang Qiu, Kai-Wei Chang, Song-Chun Zhu, Oyvind Tafjord, Peter Clark, and Ashwin Kalyan. Learn to explain: Multimodal reasoning via thought chains for science question answering. *NeurIPS*, 35:2507–2521, 2022. 7, 15, 16
- [52] Gen Luo, Yiyi Zhou, Yuxin Zhang, Xiawu Zheng, Xiaoshuai Sun, and Rongrong Ji. Feast your eyes: Mixture-of-resolution adaptation for multimodal large language models. *arXiv preprint arXiv:2403.03003*, 2024. 3
- [53] Junhua Mao, Jonathan Huang, Alexander Toshev, Oana Camburu, Alan L Yuille, and Kevin Murphy. Generation and comprehension of unambiguous object descriptions. In *CVPR*, pages 11–20, 2016. 16
- [54] Kenneth Marino, Mohammad Rastegari, Ali Farhadi, and Roozbeh Mottaghi. Ok-vqa: A visual question answering benchmark requiring external knowledge. In *CVPR*, pages 3195–3204, 2019. 16
- [55] Ahmed Masry, Xuan Long Do, Jia Qing Tan, Shafiq Joty, and Enamul Hoque. Chartqa: A benchmark for question answering about charts with visual and logical reasoning. In *ACL*, pages 2263–2279, 2022. 7, 8, 15, 16, 19
- [56] Minesh Mathew, Viraj Bagal, Rubèn Tito, Dimosthenis Karatzas, Ernest Valveny, and CV Jawahar. Infographicvqa. In *WACV*, pages 1697–1706, 2022. 7, 8, 15, 16, 18
- [57] Minesh Mathew, Dimosthenis Karatzas, and CV Jawahar. Docvqa: A dataset for vqa on document images. In *WACV*, pages 2200–2209, 2021. 7, 8
- [58] Nitesh Methani, Pritha Ganguly, Mitesh M Khapra, and Pratyush Kumar. Plotqa: Reasoning over scientific plots. In *WACV*, pages 1527–1536, 2020. 15, 16
- [59] Anand Mishra, Shashank Shekhar, Ajeet Kumar Singh, and Anirban Chakraborty. Ocr-vqa: Visual question answering by reading text in images. In *ICDAR*, pages 947–952, 2019. 15, 16
- [60] Maxime Oquab, Timothée Darcet, Theo Moutakanni, Huy V. Vo, Marc Szafraniec, Vasil Khalidov, Pierre Fernandez, Daniel Haziza, Francisco Massa, Alaaeldin El-Nouby, Russell Howes, Po-Yao Huang, Hu Xu, Vasu Sharma, Shang-Wen Li, Wojciech Galuba, Mike Rabbat, Mido Assran, Nicolas Ballas, Gabriel Synnaeve, Ishan Misra, Herve Jegou, Julien Mairal, Patrick Labatut, Armand Joulin, and Piotr Bojanowski. Dinov2: Learning robust visual features without supervision, 2023. 3
- [61] Alec Radford, Jong Wook Kim, Chris Hallacy, Aditya Ramesh, Gabriel Goh, Sandhini Agarwal, Girish Sastry, Amanda Askell, Pamela Mishkin, Jack Clark, et al. Learning transferable visual models from natural language supervision. In *International conference on machine learning*, pages 8748–8763. PMLR, 2021. 2, 3
- [62] Mike Ranzinger, Greg Heinrich, Jan Kautz, and Pavlo Molchanov. Am-radio: Agglomerative model – reduce all domains into one. Dec 2023. 3
- [63] Christoph Schuhmann, §§°romain Beaumont, Vencu Vencu, Ade Gordon, Wightman Wightman, Mehdi Cherti, Theo Coombes, Aarush Katta, Clayton Mullis, Patrick Schramowski, Srivatsa Kundurthy, Katherine Crowson, Ludwig Schmidt, Robert Kaczmarczyk, °°jenia Jitsev, UC Berkeley, and Gentec Data. Laion-5b: An open large-scale dataset for training next generation image-text models. 2
- [64] Dustin Schwenk, Apoorv Khandelwal, Christopher Clark, Kenneth Marino, and Roozbeh Mottaghi. A-okvqa: A benchmark for visual question answering using world knowledge. In *ECCV*, pages 146–162, 2022. 16

- [65] Chenglei Si, Yanzhe Zhang, Zhengyuan Yang, Ruibo Liu, and Diyi Yang. Design2code: How far are we from automating front-end engineering?, 2024. [20](#)
- [66] Oleksii Sidorov, Ronghang Hu, Marcus Rohrbach, and Amanpreet Singh. Textcaps: a dataset for image captioning with reading comprehension. In *ECCV*, pages 742–758, 2020. [16](#)
- [67] Amanpreet Singh, Vivek Natarajan, Meet Shah, Yu Jiang, Xinlei Chen, Dhruv Batra, Devi Parikh, and Marcus Rohrbach. Towards vqa models that can read. In *CVPR*, pages 8317–8326, 2019. [7](#)
- [68] Jianlin Su, Murtadha Ahmed, Yu Lu, Shengfeng Pan, Wen Bo, and Yunfeng Liu. Roformer: Enhanced transformer with rotary position embedding. *Neurocomputing*, 568:127063, 2024. [15](#)
- [69] Quan Sun, Yuxin Fang, Ledell Wu, Xinlong Wang, and Yue Cao. Eva-clip: Improved training techniques for clip at scale. *arXiv preprint arXiv:2303.15389*, 2023. [15](#)
- [70] S Svetlichnaya. Deepform: Understand structured documents at scale, 2020. [15](#), [16](#)
- [71] Hugo Touvron, Thibaut Lavril, Gautier Izacard, Xavier Martinet, Marie-Anne Lachaux, Timothée Lacroix, Baptiste Rozière, Naman Goyal, Eric Hambro, Faisal Azhar, et al. Llama: Open and efficient foundation language models. *arXiv preprint arXiv:2302.13971*, 2023. [2](#)
- [72] Penghao Wu and Saining Xie. V*: Guided visual search as a core mechanism in multimodal llms. *arXiv preprint arXiv:2312.14135*, 2023. [19](#)
- [73] Ruyi Xu, Yuan Yao, Zonghao Guo, Junbo Cui, Zanlin Ni, Chunjiang Ge, Tat-Seng Chua, Zhiyuan Liu, Maosong Sun, and Gao Huang. Llava-uhd: an lmm perceiving any aspect ratio and high-resolution images. *arXiv preprint arXiv:2403.11703*, 2024. [1](#), [2](#), [3](#), [7](#)
- [74] Zhenhua Xu, Yujia Zhang, Enze Xie, Zhen Zhao, Yong Guo, Kenneth KY Wong, Zhenguo Li, and Hengshuang Zhao. Drivegpt4: Interpretable end-to-end autonomous driving via large language model. *arXiv preprint arXiv:2310.01412*, 2023. [2](#)
- [75] Jiabo Ye, Anwen Hu, Haiyang Xu, Qinghao Ye, Ming Yan, Yuhao Dan, Chenlin Zhao, Guohai Xu, Chenliang Li, Junfeng Tian, et al. mplug-docowl: Modularized multimodal large language model for document understanding. *arXiv preprint arXiv:2307.02499*, 2023. [7](#)
- [76] Jiabo Ye, Anwen Hu, Haiyang Xu, Qinghao Ye, Ming Yan, Guohai Xu, Chenliang Li, Junfeng Tian, Qi Qian, Ji Zhang, et al. Ureader: Universal ocr-free visually-situated language understanding with multimodal large language model. *arXiv preprint arXiv:2310.05126*, 2023. [5](#), [7](#)
- [77] Qinghao Ye, Haiyang Xu, Jiabo Ye, Ming Yan, Haowei Liu, Qi Qian, Ji Zhang, Fei Huang, and Jingren Zhou. mplug-owl2: Revolutionizing multi-modal large language model with modality collaboration. *arXiv preprint arXiv:2311.04257*, 2023. [7](#)
- [78] Licheng Yu, Patrick Poirson, Shan Yang, Alexander C Berg, and Tamara L Berg. Modeling context in referring expressions. In *ECCV*, pages 69–85, 2016. [16](#)
- [79] Hang Zhang, Xin Li, Lidong Bing, and at al. Video-llama: An instruction-tuned audio-visual language model for video understanding. *arXiv preprint arXiv:2306.02858*, 2023. [2](#)
- [80] Pan Zhang, Xiaoyi Dong Bin Wang, Yuhang Cao, Chao Xu, Linke Ouyang, Zhiyuan Zhao, Shuangrui Ding, Songyang Zhang, Haodong Duan, Hang Yan, et al. Internlm-xcomposer: A vision-language large model for advanced text-image comprehension and composition. *arXiv preprint arXiv:2309.15112*, 2023. [2](#), [8](#)
- [81] Lianmin Zheng, Wei-Lin Chiang, Ying Sheng, Siyuan Zhuang, Zhanghao Wu, Yonghao Zhuang, Zi Lin, Zhuohan Li, Dacheng Li, Eric Xing, et al. Judging llm-as-a-judge with mt-bench and chatbot arena. *NeurIPS*, 36, 2024. [16](#)
- [82] Deyao Zhu, Jun Chen, Xiaoqian Shen, Xiang Li, and Mohamed Elhoseiny. Minigpt-4: Enhancing vision-language understanding with advanced large language models. *arXiv preprint arXiv:2304.10592*, 2023. [1](#), [2](#), [3](#)
- [83] Fengbin Zhu, Wenqiang Lei, Fuli Feng, Chao Wang, Haozhou Zhang, and Tat-Seng Chua. Towards complex document understanding by discrete reasoning. In *Proceedings of the 30th ACM International Conference on Multimedia*, pages 4857–4866, 2022. [15](#), [16](#)

A Appendix

A.1 Implementation Details

Training Datasets. Table 5 shows the details construction of the pretraining data of HiRes-LLaVA. Specifically, it has 1.2M captioning including original LLaVA-Pretrain datasets [44] with 558K images which is the short caption data and 708k long captioning data from ALLAVA [7]. The 0.4M OCR data are all sampled from SynthDoG [27] including 300k English OCR data and 100k Chinese OCR data.

Table 6 shows the detailed construction of the instruction tuning dataset. First, we remove 23K caption data from original LLaVA-158K [47] and include GPT4V-generated caption data, i.e., LAION-GPT4v [30] and ShareGPT4V [9]. We also sampled 406K instruct data from ALLAVA instruction data [7]. To enhance the common knowledge of our model, we convert the visual dialog [16], visual spatial reasoning [43], AI2D [26], and Science QA [51] training set into the instruct-tuning data. Finally, we collect document-oriented data from diverse datasets, includes ChartQA [55], DVQA [25], PlotQA [58], OCRVQA [59], ST-VQA [5], DocVQA [14], InfoVQA [56], DeepForm [70], TAT-DQA [83], TableFact [10] and WebSRC [12].

Module Design Details. The self-mining sampler consists of one cross-attention block with an output layer norm. The cross-attention block has a cross-attention layer and a FFN. Both of them apply the shortcut. The cross-attention layer has two layer norm for the query and key/value, respectively. As for the SliceRestore Adapter, the parameters of the self-attention layer with the layer norm are initialized from the pretrained CLIP self-attention at the same layer. To provide the positional information between slices, we apply a 2D RoPE [68, 69] on the global fusion module.

Evaluation Details. We utilize the open-source evaluation tools, lmms-eval [33], to align our evaluation method to LLaVA-Next [45]. Note that the LLaVA-W is evaluated under GPT4-0613 because of the deactivation of GPT4-0314.

Task	Dataset	# Samples
Caption	LLaVA-Pretrain	558k
	ALLAVA	708k
OCR	SynthDog-en	300k
	SynthDog-zh	100k
Total	-	1.6M

Table 5: Datasets in the pretraining stage.

A.2 More Visualization

Samples from EntityGrid-QA Benchmark. We illustrate three examples from our proposed EntityGrid-QA benchmark in Fig. 6. These three samples visualize examples of the three tasks in the benchmark we proposed. For each task, we write or paste the digital number or object directly onto each position of an empty image, and ask questions to the models.

More Qualitative Results. To further validate the effectiveness of our model, we illustrate the more qualitative results of InfoVQA, ChartQA and V* Benchmark in Fig. 7 and Fig. 8. Moreover, we give two qualitative examples to present the HiRes-LLaVA’s capability of generating HTML code when given a website image in Fig. 9.

A.3 Broader Impacts

The development of HiRes-LLaVA advances the field of vision-language models and has broad implications for various applications, including document analysis, medical imaging and remote sensing. However, alongside these potential benefits, there are considerable concerns.

HiRes-LLaVA, not having undergone rigorous safety training, might generate harmful or inappropriate content, leading to legal and ethical issues. Furthermore, its enhanced ability to process high-resolution inputs could be misused for creating misleading news, contributing to disinformation.

Task	Dataset	# Sample
Captioning	ShareGPT4V [9]	91K
	TextCaps [66]	22K
	Laion-GPT4V [30]	11K
General QA	VQAv2 [20]	83K
	GQA [24]	72K
	OKVQA [54]	9K
	A-OKVQA [64]	66K
	Visual Spatial Reasoning [43]	12K
	VisualDialog [16]	123K
Science	AI2D [26]	4K
	ScienceQA [51]	12K
Doc QA	ChartQA [55]	28K
	DVQA [25]	10K
	PlotQA [58]	10K
	OCRVQA [59]	80K
	ST-VQA [5]	18K
	DocVQA [14]	49K
	InfoVQA [56]	14K
	DeepForm [70]	5K
	TAT-DQA [83]	2K
	TableFact [10]	14K
WebSRC [12]	5K	
Grounding	RefCOCO [78, 53]	48K
	VG [29]	86K
Conversations	LLaVA [47]	135K
	ALLaVA [7]	400K
HTML Code Generation	WebSight [31]	50K
Text-only	ShareGPT [81]	40K
Total	-	1.5M

Table 6: Summary of datasets used in the instruction tuning stage.

These potential negative impacts highlight the need for careful management and ethical guidelines in the deployment of such technologies.

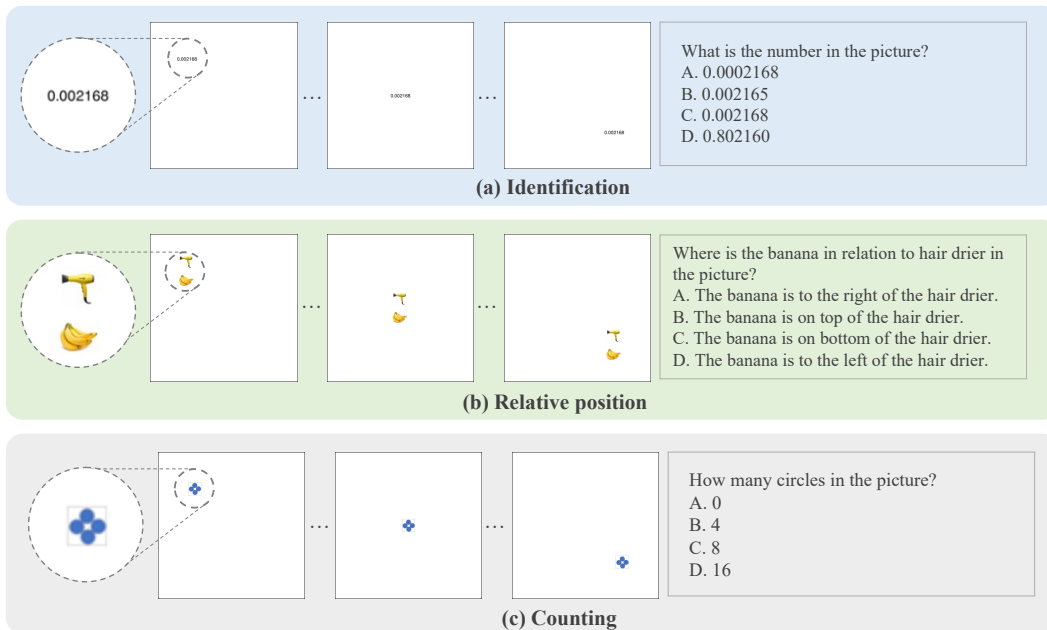
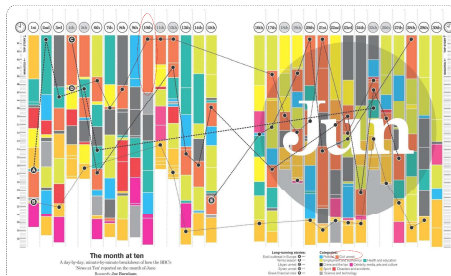


Figure 6: Examples of our proposed EntityGrid-QA Benchmark.



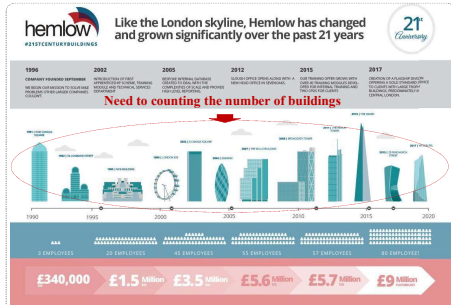
Q: What category was the *top story* on the 10th of June?

LLaVA-1.6: politics ✗ Monkey: politics ✗
Ours: civil unrest ✓



Q: Which environment issue is mentioned in the bottom row of the bulb image in the infographic?

LLaVA-1.6: waste ✗ Monkey: pollution ✗
Ours: ocean pollution ✓



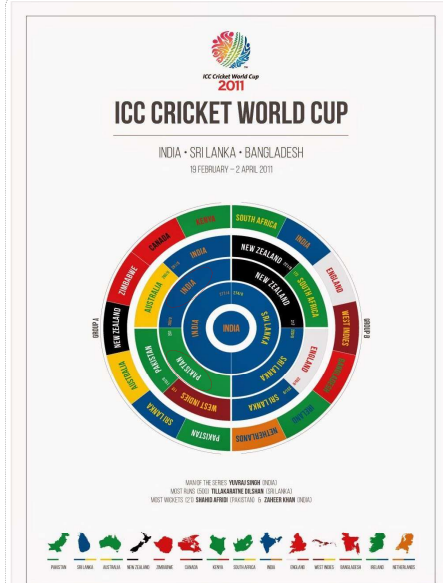
Q: How many buildings were constructed by Hemlow?

LLaVA-1.6: 21 ✗ Monkey: 9 ✗
Ours: 12 ✓



Q: What is the *third ingredient* listed to make Pasta?

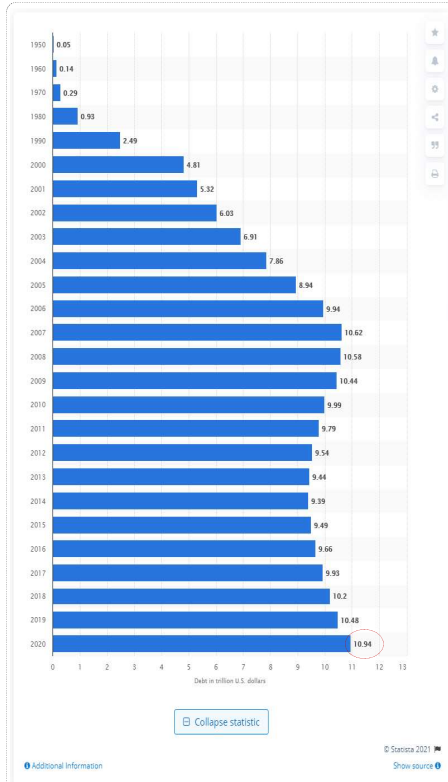
LLaVA-1.6: water ✗ Monkey: eggs ✗
Ours: salt ✓



Q: Who was the *opponent of India* in the semifinals of World Cup 2011?

LLaVA-1.6: england ✗ Monkey: sri lanka ✗
Ours: pakistan ✓

Figure 7: Qualitative results from InfoVQA [56].



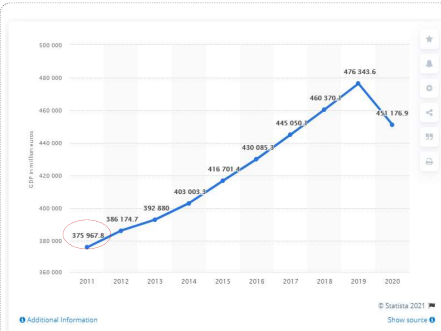
Q: What was the mortgage debt in the United States in 2020?

LLaVA-1.6: 10.4 ✗ Monkey: 12.13 ✗
Ours: 10.94 ✓



Q: What is the color of *the woman's scarf*?
(A) white
(B) red
(C) yellow
(D) green

LLaVA-1.6: A ✗ Monkey: A ✗
Ours: B ✓



Q: What was Belgium's GDP in 2011?

LLaVA-1.6: 37596.8 ✗
Monkey: 386174.7 ✗
Ours: 375967.8 ✓



Q: What is the *cartoon character* on the clock.
(A) Bugs Bunny
(B) Mickey Mouse
(C) SpongeBob
(D) Donald Duck

LLaVA-1.6: C ✗ Monkey: A ✗
Ours: B ✓

Figure 8: Qualitative results from ChartQA [55] and Vstar Benchmark [72]. We use the red circle to highlight the answer target in the image.

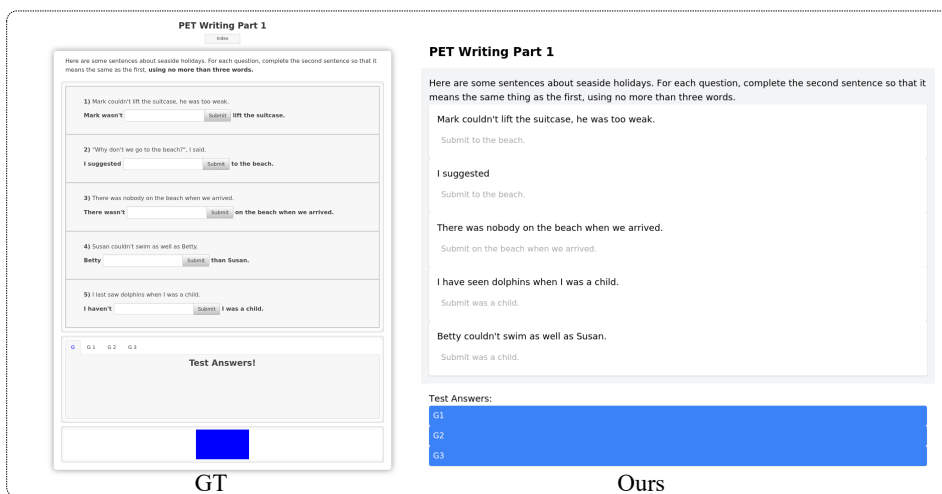
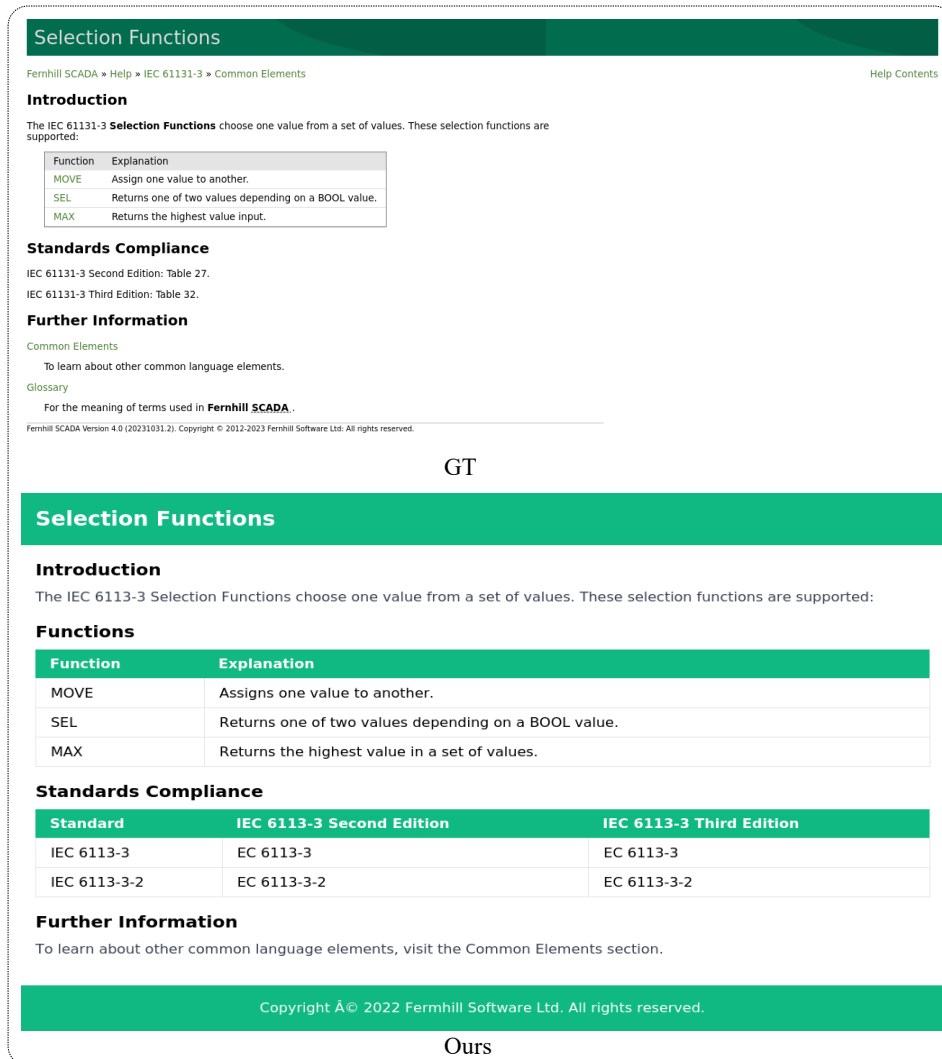


Figure 9: **Qualitative results on Image2HTML task [65].** We visualize convert the generated html code to website image and compare to the input image.